
HALO: Hadamard-Assisted Lossless Optimization for Efficient Low-Precision LLM Training and Fine-Tuning

Saleh Ashkboos^{*1} Mahdi Nikdan^{*2} Soroush Tabesh^{*2} Roberto L. Castro² Torsten Hoefer¹ Dan Alistarh^{2,3}

Abstract

Quantized training of Large Language Models (LLMs) remains an open challenge, as maintaining accuracy while performing all matrix multiplications in low precision has proven difficult. This is particularly the case when *fine-tuning pre-trained models*, which often already have large weight and activation outlier values that render quantized optimization difficult. We present HALO, a novel quantization-aware training approach for Transformers that enables accurate and efficient low-precision training by combining 1) strategic placement of Hadamard rotations in both forward and backward passes, to mitigate outliers during the low-precision computation, 2) FSDP integration for low-precision communication, and 3) high-performance kernel support. Our approach ensures that all large matrix multiplications during the forward and backward passes are executed in lower precision. Applied to LLAMA-family models, HALO achieves near-full-precision-equivalent results during fine-tuning on various tasks, while delivering up to $1.31\times$ end-to-end speedup for full fine-tuning on RTX 4090 GPUs. Our method supports both standard and parameter-efficient fine-tuning (PEFT) methods, both backed by efficient kernel implementations. Our results demonstrate the first practical approach to fully quantized LLM fine-tuning that maintains accuracy in FP8 precision, while delivering performance benefits.

1. Introduction

The high performance of large language models (LLMs) across a wide series of tasks comes with considerable computational costs for both inference and training. Reducing

^{*}Equal contribution ¹ETH Zurich ²ISTAustria ³Neural Magic. Correspondence to: Saleh Ashkboos <saleh.ashkboos@inf.ethz.ch>, Torsten Hoefer <thor@ethz.ch>, Dan Alistarh <dan.alistarh@ista.ac.at>.

Preprint.

these costs is currently one of the key directions in Machine Learning Systems research (Dao, 2023a; Flashinfer.ai, 2023; Kwon et al., 2023; Ashkboos et al., 2024a).

For *LLM inference*, a standard acceleration approach has been the *quantization* of weights and activations, which reduces the precision at which they are stored and potentially also computed over, e.g. (Frantar et al., 2022; Xiao et al., 2023; Zhao et al., 2023b; Ashkboos et al., 2023; Chee et al., 2024; Tseng et al., 2024; Ashkboos et al., 2024b).

By contrast, much less is known about quantization in the context of *LLM training*. Concretely, although we have fast hardware support for low-precision matrix multiplications in INT8/FP8 and even INT4 (NVIDIA, 2017), it is currently not clear how to stably and efficiently train or fine-tune large-scale models using only low-precision operations (Wortsman et al., 2023; Xi et al., 2024b). Intuitively, this is because efficient and accurate quantized training is much more challenging than quantized inference: for full acceleration, all three matrix multiplications occurring during training (one during the forward pass and two during back-propagation) must be executed in lower precision. In turn, this creates critical issues both in terms of *accuracy*—as quantizing weights, activations, and errors can induce significant training instability—but also in terms of *performance*—as the overheads of switching between representations can negate the performance gains of lower-precision computation.

Moreover, the problem becomes especially challenging when *fine-tuning a pre-trained model*. In this case, it is well-known that models already have large (and structured) outliers in the weight, activation, and error distributions (Wei et al., 2022; Xiao et al., 2023; Sun et al., 2024; Nrusimha et al., 2024), which makes stable training harder to achieve compared to the initial pre-training of LLMs.

Contributions. In this paper, we present HALO, a new quantized training technique which modifies the structure of Transformer-based models (Vaswani, 2017) in a transparent fashion, allowing them to be trained in lower precision (FP8, INT8, or even FP6), with minimal accuracy loss. Importantly, we do so while performing *all large matrix multiplications*, for both the forward- and backward-pass, in lower

arXiv:2501.02625v1 [cs.LG] 5 Jan 2025

precision both for fine-tuning, and for parameter-efficient fine-tuning (PEFT).

HALO starts from an in-depth analysis of the sensitivity of different data types (weight, input, and output gradients) during back-propagation (LeCun et al., 2002). This leads to using varying numbers of Hadamard transformations and defining multiple levels for HALO based on the required precision, data format, and acceptable accuracy drop during training. We complement these algorithmic contributions with efficient kernel support, showing computational speedups. In addition, we integrate our scheme with the Fully Sharded Data Parallel (FSDP) scheme to enable further savings by performing low-precision communication.

In practice, our implementation of HALO, currently focused on efficiency for consumer-grade NVIDIA 4090 GPUs, can closely track the full-precision baseline for INT8-only fine-tuning of pre-trained LLAMA-family models (Dubey et al., 2024), with a $1.29\times$ end-to-end speedup, across challenging generation and reasoning tasks, offering a superior accuracy-performance trade-off to prior methods (Wortsman et al., 2023; Xi et al., 2024b). We also obtain lossless fine-tuning in FP8, with a $1.31\times$ speedup.

In summary, our contributions are as follows:

- We consider the challenging problem of quantized fine-tuning of a pre-trained model using only lower-precision multiplications, and analyze the quantization errors during the process due to outliers across various dimensions.
- Based on our analysis, we propose using left- and right-hand-side Hadamard transforms to address outliers over matrix rows and columns, respectively. We show how they can be inserted “strategically” in the Transformer architecture for both forward and backward passes, minimizing overheads.
- We then, explore different “outlier protection” levels for HALO based on the number and placement of Hadamard transformations during training: intuitively, HALO-0 does not employ any Hadamard rotations, HALO-2 employs rotations to protect *all multiplications* on the forward and backward passes, while HALO-1 strikes a trade-off between accuracy and performance. These levels are independent of the precision used during fine-tuning, which enables us adjust them to recover final accuracy, while maximizing end-to-end speedup.
- HALO is compatible with *full fine-tuning (FFT)* and *PEFT methods*, and is backed by efficient GPU implementations, currently aimed at NVIDIA RTX GPUs. Moreover, the fact that all computation happens in quantized form offers the opportunity to also perform

quantized communication during sharded (FSDP) training, which we implement as well.

- We examine the accuracy and performance of HALO for fine-tuning LLAMA-family models (Dubey et al., 2024), via both FFT and PEFT. We observe that HALO closely tracks the accuracy of full-precision variants across a wide series of tasks, matching or improving upon prior work (Wortsman et al., 2023; Xi et al., 2024b), especially in the more lossy INT8 and FP6 formats. We provide performance measurements per module, per multiple blocks, and end-to-end peak speedups of $1.58\times$, $1.37\times$, and $1.29\times$ for INT8, and $1.67\times$, $1.37\times$, and $1.31\times$ for FP8, respectively.

Overall, our results show that it is possible to perform the majority of the forward-backward computation (all linear modules) in lower precision accurately and performantly, even if the model already has an inherent outlier structure in weights, activations, and errors.

2. Related Work

Most quantization methods focus on applying quantization for inference, with the objective of compressing the model through weight-only quantization (Frantar et al., 2022; Dettmers et al., 2023; Egiazarian et al., 2024; Tseng et al., 2024) or accelerating inference by jointly quantizing both weights and activations, thus performing the majority of computations in lower precision (Zhao et al., 2023b; Ashkboos et al., 2023; Dettmers et al., 2022; Xiao et al., 2023; Ashkboos et al., 2024b; Liu et al., 2024). Specifically, it has been observed that activation quantization is challenging due to the presence of outlier features (Wei et al., 2022), and recent works focus on applying light-weight transformations to mitigate such features on top of pre-trained models. Specifically, QuaRot (Ashkboos et al., 2024b) mitigates outliers by applying (randomized) Hadamard rotations to weight and activation matrices, allowing most inference computations to be performed in 4 bits. SpinQuant (Liu et al., 2024) employs a similar base idea, but *trains* a subset of the orthogonal transformations.

While LLM inference benefits from quantization, performing low-precision computation during the *backward pass* is challenging due to the wide dynamic range of errors (gradients with respect to layer outputs) (Micikevicius et al., 2017; Chitsaz et al., 2024). LM-FP8 (Peng et al., 2023) trains large-scale models from scratch using FP8 on 40-100B of tokens. Fishman et al. (2024) demonstrates that FP8 training becomes unstable when training with over $>250B$ tokens, and proposes a new activation function in the MLP to address this issue. Thus, their technique cannot easily be extended to fine-tuning an already trained model.

Integer quantization is another promising direction due to its

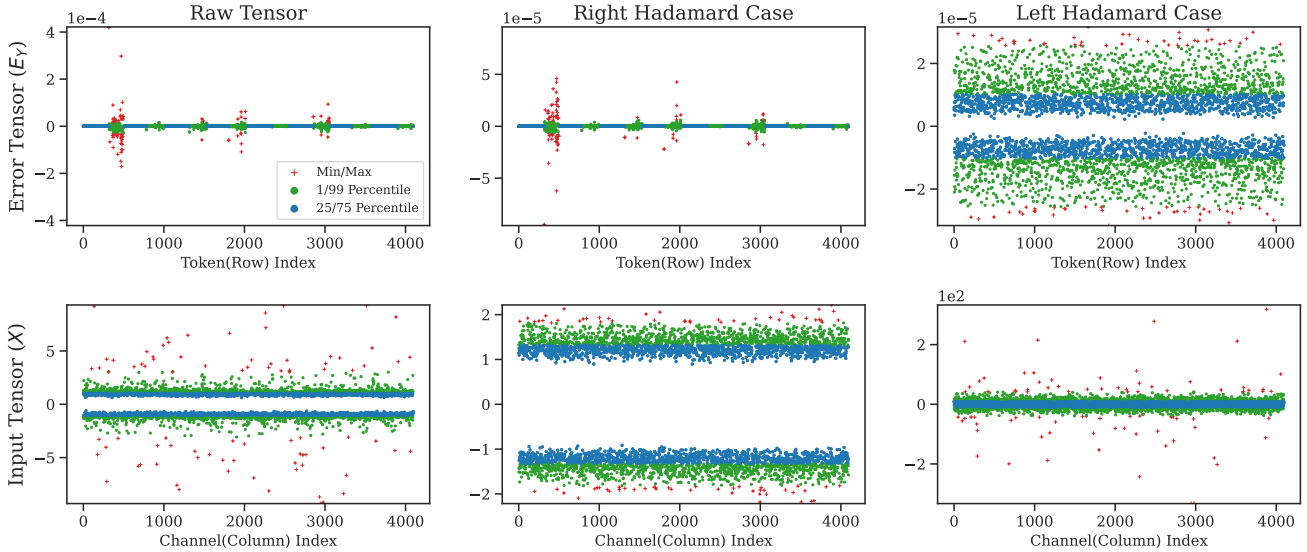


Figure 1. Largest magnitudes of output gradients, or errors (first row), and the inputs (second row) of the key projection (`k_proj`) (4096 channels) in the 10-th layer of LLaMA3-8B model over 4096 tokens (batch-size 4 with 1024 sequence length) in the 60th step of the ViGGO fine tuning. The outliers are propagated across channels(columns) in the output gradient matrix (errors) and across tokens(rows) in the input matrix, and can be mitigated after applying Left- and Right-Hadamard transformations, respectively.

easy and efficient implementation in hardware (Baalen et al., 2023), though it comes at the cost of a narrower dynamic range. SwitchBack (Wortsman et al., 2023) quantizes two out of three matrix multiplications in the linear modules using INT8, while retaining the third in high precision for vision models with up to 1B parameters. Jetfire (Xi et al., 2024b) proposes a more complex 2D block-wise quantization approach to address this issue when training from scratch in INT8, albeit with large quantization overhead for small ($< 1\text{B}$ -parameter) models. On the one hand, Jetfire obtains good accuracy and significant end-to-end speedups and memory reductions (1.4-1.5x); on the other, their method was not tested for fine-tuning, and modifying the data flow to INT8 comes with significant implementation challenges.

We compare to both JetFire and SwitchBack as our main baselines, in the context of fine-tuning. We obtain similar or higher accuracy than SwitchBack, while consistently outperforming it in terms of runtime, since we execute all multiplications in low precision. Relative to JetFire, we obtain generally higher accuracy, with similar speedups; on this last point, we note that performing an apples-to-apples comparison is difficult in this case, due to their different-precision dataflow.

While the above works mainly focus on accurate training from scratch, efficient fine-tuning is another critical workload involving the backward pass to update the parameters of a pre-trained model for a specific task. Although most recent work focuses on making fine-tuning more efficient by reducing memory usage (Dettmers et al., 2024; Nikdan

et al., 2024) through PEFT-style schemes (Hu et al., 2021), accelerating actual computation during fine-tuning remains an unexplored area.

Relative to prior work such as SwitchBack and Jetfire, we consider a related but more challenging problem. Since we focus on accelerated lower-precision fine-tuning of *pre-trained models*, the outlier structure of the model is already formed, and our scheme has to mitigate it across all matrix multiplications. Moreover, we present the first in-depth analysis of quantization errors across inputs, weights, and errors in the forward and backward passes. Based on this analysis, we define multiple levels of outlier mitigation to optimize the *accuracy-performance* tradeoff for a given training setting. We present efficient implementation for low-precision matrix multiplication as well as quantized communication. Finally, we develop our scheme to accelerate both full and PEFT-style fine-tuning and show almost no accuracy degradation on challenging tasks for fine-tuning large-scale models (with 7-8B parameters).

3. Background

Linear Layers. Let matrices $\mathbf{W} \in \mathbb{R}^{n \times m}$, $\mathbf{X} \in \mathbb{R}^{b \times m}$ and $\mathbf{Y} \in \mathbb{R}^{b \times n}$ be the weights, inputs, and outputs of an $n \times m$ linear layer acting on an input with batch size b . The forward and backward passes include the following matrix-matrix multiplications, in PyTorch notation (Paszke et al., 2019):

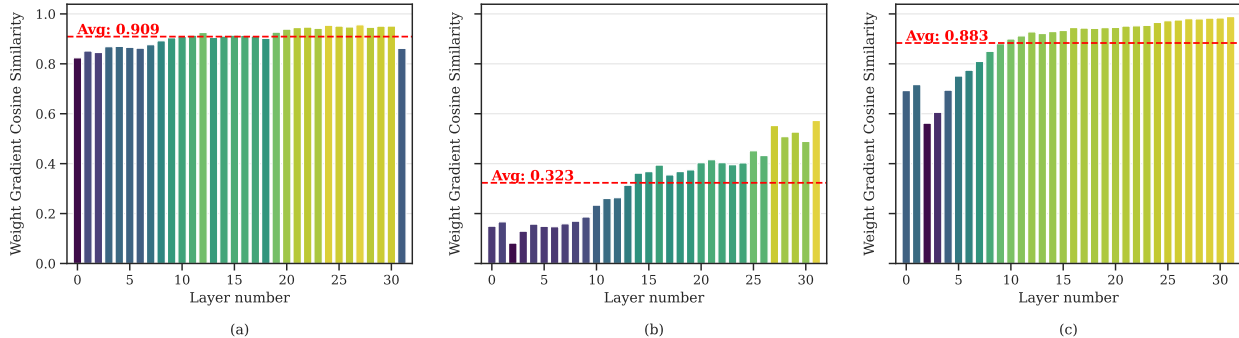


Figure 2. Cosine similarity between the weight gradients of the baseline model (BF16) and the quantized model when quantization is applied during the (a): backward pass, (b): forward pass, and (c): forward pass with Hadamard transformation in a single fine-tuning step of LLAMA3-8B on the GSM8K dataset. Compared to the backward pass, the forward pass is more sensitive to quantization. We improve the results by applying Hadamard transformation during the forward pass ($\overset{H}{F}$). For each case, we present the weighted average (over the number of parameters) for all linear modules in each layer.

$$\mathbf{Y} = \mathbf{X} \cdot \mathbf{W}^T \quad (\text{Forward}) \quad (1)$$

$$\mathbf{G} = \mathbf{E}_Y^T \cdot \mathbf{X} \quad (\text{Gradient}) \quad (2)$$

$$\mathbf{E}_X = \mathbf{E}_Y \cdot \mathbf{W} \quad (\text{Error}) \quad (3)$$

where \mathbf{G} , \mathbf{E}_X , and \mathbf{E}_Y are the gradients w.r.t. the weights, inputs, and outputs (where the last two are known as *errors*), respectively. The first matrix multiplication occurs during the forward pass, denoted by \mathbf{F} , while the last two occur during the backward pass: one for computing the weight gradients, denoted by \mathbf{G} , and the other for computing the errors, denoted by \mathbf{E} .

Hadamard Transformations. For a given size d , a normalized Hadamard matrix \mathbf{H}_d is an orthonormal matrix where $\mathbf{H}_d \mathbf{H}_d^T = \mathbf{I}$. When $d = 2^n$, \mathbf{H}_d is called the Walsh-Hadamard matrix whose entries are $\pm \frac{1}{\sqrt{d}}$ and can be built via recursive construction $\mathbf{H}_d = \mathbf{H}_2 \otimes \mathbf{H}_{d/2}$.

Assume that we are given a matrix $\mathbf{A} \in \mathbb{R}^{d \times d}$. We define the following transformations:

- A **right-hand-side Hadamard** transformation, is the process of applying the linear transformation $\mathbf{h}(\mathbf{A}) = \mathbf{A} \mathbf{H}_d$ which could be done as a matrix-matrix multiplication. When d is power-of-two, \mathbf{H}_d is called Walsh-Hadamard, and the above transformation can be done using a recursive algorithm with $O(d \log d)$ operations (Yavne, 1968). Following (Ashkboos et al., 2024b), when d is not a power of two, we factorize it as $d = 2^n m$, where m is the size of a known Hadamard matrix. We then apply the Kronecker construction: $\mathbf{H}_d = \mathbf{H}_{2^n} \otimes \mathbf{H}_m$.
- We also use the **left-hand-side Hadamard** transformation, defined as $\mathbf{h}'(\mathbf{A}) = \mathbf{H}_d^T \mathbf{A}$, which can be calculated by transposing $\mathbf{h}(\mathbf{A}^T)$.

Outlier Mitigation. Chee et al. (2024) observes that the magnitude of the largest elements (outliers) in a matrix \mathbf{A} that we wish to quantize for inference can be reduced by applying orthogonal transformations to \mathbf{A} from both sides, a method known as *Incoherence Processing* (Chen et al., 2013). We use the Hadamard transformation to mitigate outliers and improve quantization errors during the low-precision calculations of \mathbf{F} , \mathbf{G} , and \mathbf{E} in Equations (1-3).

Ashkboos et al. (2024b) showed that applying the right-hand Hadamard $\mathbf{h}(\mathbf{A})$ can improve quantization when \mathbf{A} has outlier *columns* (columns containing entries with large magnitude), which is the case in the input tensors. Conversely, when outliers occur in *rows*, applying $\mathbf{h}'(\mathbf{A})$ can mitigate such outliers by performing the Hadamard transformation on the transposed \mathbf{A} .

Low-Precision Matrix-Multiplication. For given matrices $\mathbf{A} \in \mathbb{R}^{m \times k}$ and $\mathbf{B} \in \mathbb{R}^{k \times n}$, our goal is to perform matrix multiplication $\mathbf{Y} = \mathbf{A}_Q \mathbf{B}_Q$ in low precision, where $\mathbf{A}_Q, \mathbf{B}_Q$ are the quantized copies of \mathbf{A} and \mathbf{B} . There are different ways of introducing such transformations:

- **No Hadamard Case (denoted \mathbf{Y}):** Here, we directly apply the quantization function and perform $\mathbf{A}_Q \mathbf{B}_Q$ without using any Hadamard transformation.
- **Left Case (denoted $\overset{H}{\mathbf{Y}}$):** Here, we apply a left-hand Hadamard transformation of size m on \mathbf{A} before quantization and perform $\mathbf{H}_m (\mathbf{H}_m^T \mathbf{A})_Q \mathbf{B}_Q$. To (approximately) cancel out the transformation (due to quantization error), we apply a left-hand Hadamard transformation on the output of the low-precision matrix multiplication.
- **Right Case (denoted $\overset{H}{\mathbf{Y}^H}$):** We apply a right-hand Hadamard transformation of size n on \mathbf{B} and perform $\mathbf{A}_Q (\mathbf{B} \mathbf{H}_n)_Q \mathbf{H}_n^T$.

- **Middle Case (denoted $\overset{\text{H}}{\mathbf{Y}}$):** Here, we apply Hadamard transformations of size k from the right to \mathbf{A} and from the left to \mathbf{B} and perform $(\mathbf{A}\mathbf{H}_k)_Q(\mathbf{H}_k^T\mathbf{B})_Q$.

QuaRot (Ashkboos et al., 2024b) applies the middle case to Equation (1), which we will denote by $\overset{\text{H}}{\mathbf{F}}$. This could be done efficiently, especially when k is a power of two. In this case, we transform the weights offline and apply a Walsh-Hadamard transformation to the inputs during inference.

Full and Parameter-Efficient Fine-Tuning. Full fine-tuning (FFT) happens on a pre-trained model and involves adjusting all model parameters on a downstream task. Due to memory constraints, this is often infeasible for LLMs on consumer hardware. Parameter-efficient fine-tuning (PEFT) methods focus on reducing memory usage during fine-tuning. Low-Rank Adaptation (LoRA) (Hu et al., 2021) is the most common PEFT method. A LoRA linear layer is parameterized by a non-trainable weight matrix $\mathbf{W} \in \mathbb{R}^{n \times m}$, as well as trainable components $\mathbf{U} \in \mathbb{R}^{r \times m}$ and $\mathbf{V} \in \mathbb{R}^{n \times r}$ with small r (usually between 8 and 64). A LoRA linear module includes the following operations:

$$\mathbf{Y} = \mathbf{X} \cdot \mathbf{W}^T + (\mathbf{X} \cdot \mathbf{U}^T) \cdot \mathbf{V}^T, \quad (4)$$

$$\mathbf{E}_X = \mathbf{E}_X^{UV} + \mathbf{E}_X^W = (\mathbf{E}_Y \cdot \mathbf{V}) \cdot \mathbf{U} + \mathbf{E}_Y \cdot \mathbf{W}, \quad (5)$$

$$\mathbf{G}_V = \mathbf{E}_Y^T \cdot (\mathbf{X} \cdot \mathbf{U}^T), \quad (6)$$

$$\mathbf{G}_U = (\mathbf{V}^T \cdot \mathbf{E}_Y^T) \cdot \mathbf{X}, \quad (7)$$

where \mathbf{G}_U and \mathbf{G}_V are the gradients of \mathbf{U} and \mathbf{V} , respectively. We note that since low-rank operations are relatively fast, our goal is to quantize matrix multiplications where the low-rank matrices \mathbf{U} and \mathbf{V} are not involved.

4. Method

In this section, we describe our proposed HALO method for low-precision fine-tuning of a pre-trained model. First, we look at how the use of left- and right-hand Hadamard transformations can address outlier issues in activations and errors during fine-tuning. Then, we study the challenges of fine-tuning large models in low precision and motivate our design choices in HALO. Specifically, we discuss different *levels* (variants) of HALO that employ various numbers of Hadamard transformations and describe how HALO is used during full fine-tuning (FFT) and parameter-efficient fine-tuning (PEFT). Finally, we discuss the details of implementing our schemes for performing low-precision matrix multiplication and communication.

4.1. Hadamard Transformation for Outlier Mitigation

To address the existence of outlier values in the matrices,¹ HALO applies the Hadamard transformation before quantization. However, activation and error tensors can exhibit different outlier structures during fine-tuning; thus, the transformations we apply are also different.

Specifically, in activation tensors \mathbf{X} , there are a few columns of significantly larger magnitude (Liu et al., 2024), resulting in propagated outliers *across rows* (token/batch dimension). Since the right-hand Hadamard transformation rotates the input rows (Ashkboos et al., 2024b), applying $\mathbf{h}(\mathbf{X})$ mitigates outliers in the activation matrix \mathbf{X} . However, in error tensors \mathbf{E}_X , unlike activation tensors, the outliers are propagated *across columns* (channel/feature dimension). Thus, we apply the left-hand Hadamard transformation, or $\mathbf{h}'(\mathbf{E}_Y)$, which mitigates the error outliers by rotating the column vectors. Figure 1 illustrates the effect of applying $\mathbf{h}(\mathbf{X})$ and $\mathbf{h}'(\mathbf{E}_Y)$ on both the input and error tensors in the Key Projection (`k_proj`) layer. We observe some outlier rows (tokens) in the error tensor (top row) that are not resolved by applying right-hand Hadamard transformations (top-middle plot). However, the outlier issue is resolved by applying left-hand Hadamard transformations to these tensors (top-right plot). However, for the input tensors (bottom row), the outlier issues are successfully addressed by applying right-hand Hadamard transformations (bottom-middle plot).

4.2. Challenges of Low-Precision Fine-Tuning

One can apply left, right, or middle cases of the Hadamard transformations for low-precision calculations of Equations (1-3). Any combination of these cases can be applied, resulting in 24 different modes (including the "No-Hadamard" case) for using such transformations. In this section, we study the effect of quantization on the forward and backward passes to identify the most sensitive parts during fine-tuning. Then, we examine the implementation aspects of using quantization during fine-tuning to select the scheme that provides the highest accuracy while minimizing overhead in computation, memory, and communication.

Forward Vs. Backward Quantization. Previous work has shown that activations (\mathbf{X}) and errors (\mathbf{E}_Y) contain outliers in their columns and rows, respectively (Ashkboos et al., 2024b; Xiao et al., 2023; Xi et al., 2023; Chitsaz et al., 2024). However, it remains unclear which matrix multiplication is more sensitive to quantization during fine-tuning. We study the cosine similarity between the weight gradients of the baseline model (no quantization) and the quantized model when quantization is applied during the forward pass

¹Outliers can be roughly defined as values ≥ 10 larger than the value average in the considered tensor.

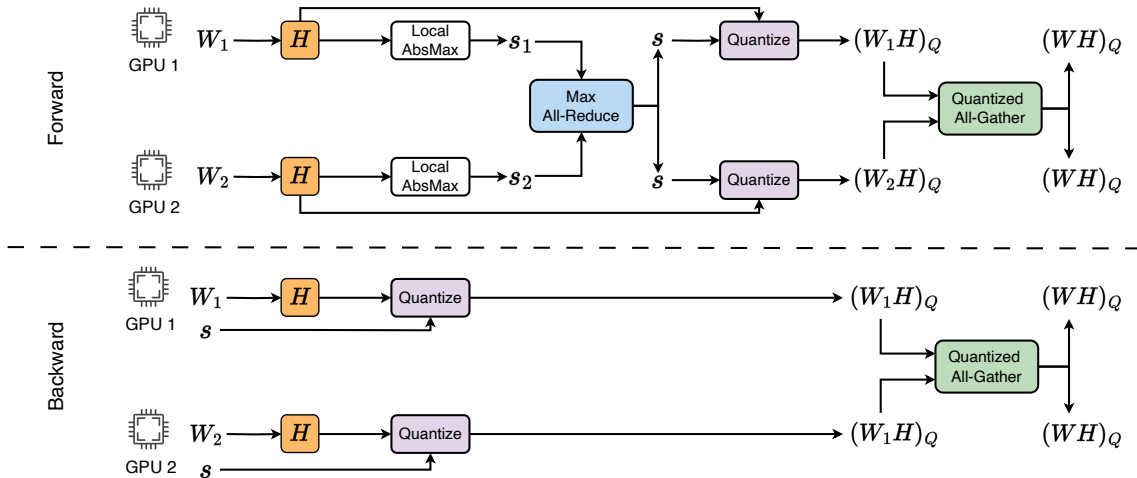


Figure 3. Forward and backward passes in HQ-FSDP for two GPUs: During the **forward pass**, each GPU performs a right-hand Hadamard transformation and computes the absolute maximum (AbsMax) s_i over its local weight shard W_i . Then, all GPUs participate in an **All-Reduce** operation and compute the global maximum absolute value s . Each GPU uses this global value to quantize its own weight shard. Finally, an **All-Gather** operation is performed on the quantized shards $(W_i H)_Q$. In the **backward pass**, all GPUs apply a right-hand Hadamard transformation and then use s (stored from forward) to quantize their shards before quantized communication. Notably, since the master weights are stored in higher precision, keeping the quantized shard for the backward pass would consume additional memory. Therefore, the quantized weights are recomputed during the backward pass instead.

(Equation 1) or the backward pass (Equations 2-3).

Figure 2 shows that the computed weight gradients have significantly lower cosine similarity² to the baseline model when quantization is applied during the forward pass. In the former case, where we quantize the backward pass and keep the forward pass in BF16 as the baseline model, the averaged cosine similarity is 0.909. However, when we apply the quantization to the forward pass (Equation 1) and keep the backward unchanged, the average cosine similarity drops from 0.909 to 0.323. This may be due to larger quantization errors in the activations (caused by larger outliers) or errors that occur during the network loss calculation after quantizing the forward pass.

We conclude that mitigating outliers is more critical during the forward pass, and we can recover most of the averaged cosine similarity (0.883) by applying Hadamard transformations during the forward pass on the weights and inputs as in QuaRot (Ashkboos et al., 2024b).

FSDP Integration. Fully Sharded Data Parallel (FSDP) (Zhao et al., 2023a) is a common distributed training strategy for LLM fine-tuning. In FSDP, model weights are *sharded* (i.e., distributed) across multiple GPUs. Whenever necessary, a subset of the weights (typically corresponding to a transformer block) is *all-gathered*, enabling every GPU to have the full weight subset required for an operation. This

²A flattened concatenation of all gradients was used for measuring cosine similarity.

communication occurs before the forward and backward passes of each block. After the backward pass, gradients are *reduce-scattered*, ensuring that each process maintains the averaged gradient for its own shard (Figure 3).

Since HALO requires only the quantized weights for performing the **F** and **E** operations, it allows for low precision all-gather communications. We refer to this approach as Hadamard-Quantized FSDP (HQ-FSDP) and implement it as follows: (a) if necessary, each process applies a right-hand Hadamard transformation to its shard (depending on the HALO level implemented), (b) each process computes a local quantization scale for its shard, (c) the scales are max-reduced to ensure that every process has the global scale per weight matrix, (d) each process quantizes its shard with the global scales, and (e) the low-precision quantized weights are communicated. This approach significantly reduces communication overhead while distributing the quantization and, possibly, the Hadamard transformation overhead across processes. Notably, the global scales calculated during the forward pass are reused in the backward pass, skipping steps (b) and (c) above. More implementation details are included in the Appendix A.1.

FSDP is often combined with Activation Checkpointing (AC), which saves only selected activations (*checkpoints*, e.g., before and after transformer blocks) during the forward pass, reducing memory usage. Before the backward pass of each block, intermediate activations are recomputed via a second forward pass. With AC, FSDP communicates

each weight only once during the backward pass, reusing it for both the second forward pass and the backward pass. Thus, when using HQ-FSDP with AC, applying the same Hadamard transformation to the weights in both \mathbf{F} and \mathbf{E} operations is essential to ensure communication speedup.

Activation Quantization For Memory Reduction. Previous work (Xi et al., 2024a) has shown that up to 40% of memory is used to store activations during training in LLAMA-style models. This is because the activation tensor \mathbf{X} in Equation (1) must be stored and reused in Equation (2) during the backward pass. We always store the quantized version of \mathbf{X} for the backward pass to address this issue. When we apply a right-hand Hadamard operation on \mathbf{X} during the forward pass, we need to apply another right-hand Hadamard operation on the output of Equation (2) to ensure identical computation.

4.3. The HALO Method

Full Fine Tuning. Based on the above observations, we define a series of levels in HALO based on the Hadamard transformations we use during \mathbf{F} , \mathbf{E} , and \mathbf{G} calculations in Equations (1-3) and show the Hadamard placement in parentheses. We summarize all HALO levels and their calculations in Table 5.

1. At the first level, denoted by HALO-0(\mathbf{F} , \mathbf{E} , \mathbf{G}), we do not apply any Hadamard transformation before quantization. This scheme has no Hadamard overhead, which makes it suitable for representations with a wide dynamic range (like FP8).
2. At the next level, denoted by HALO-1($\overset{\mathbf{H}}{\mathbf{F}}$, $\mathbf{E}^{\mathbf{H}}$, $\mathbf{G}^{\mathbf{H}}$), we employ the middle case during the forward pass to mitigate issues with weight gradients (Figure 2c). Specifically, right-hand Hadamard transforms are applied to both input and weight matrices prior to quantization. As discussed in Section 4.1, this introduces two implementation concerns: 1) *Low-Precision Communication*: We apply a right-hand Hadamard transform to the weights in Equation 3 to facilitate integration with HQ-FSDP and Activation Checkpointing. 2) *Memory Reduction*: To improve memory efficiency, we apply a right-hand Hadamard transform to the input during the backward pass (Equation 2). This allows us to reuse the quantized inputs from the forward pass, eliminating the need to keep the high-precision inputs in memory.
3. Finally, to mitigate outliers in the errors, we define the highest level by applying a left-hand Hadamard transformation to \mathbf{E} , denoted by HALO-2($\overset{\mathbf{H}}{\mathbf{F}}$, $\overset{\mathbf{H}}{\mathbf{E}}$, $\mathbf{G}^{\mathbf{H}}$).

Parameter Efficient Fine Tuning. To accelerate parameter-efficient fine-tuning (PEFT), we apply ($\overset{\mathbf{H}}{\mathbf{F}}$, $\overset{\mathbf{H}}{\mathbf{E}}$, \mathbf{G}) on the

Equations (4-5) while maintaining low-rank operations (Equations 7-6) in high precision due to their inherent efficiency. In this case, the Equations (4-5) will become

$$\mathbf{Y} \approx (\mathbf{X}\mathbf{H})_{\mathbf{Q}} \cdot (\mathbf{W}\mathbf{H})_{\mathbf{Q}}^{\mathbf{T}} + (\mathbf{X}\mathbf{U}^{\mathbf{T}}) \cdot \mathbf{V}^{\mathbf{T}}, \quad (8)$$

$$\mathbf{E}_{\mathbf{X}} \approx \mathbf{E}_{\mathbf{X}}^{\mathbf{UV}} + \mathbf{H} \cdot (\mathbf{H}^{\mathbf{T}}\mathbf{E}_{\mathbf{Y}})_{\mathbf{Q}} \cdot (\mathbf{W}\mathbf{H})_{\mathbf{Q}}\mathbf{H}^{\mathbf{T}}. \quad (9)$$

We note that we apply a right-hand Hadamard transformation and quantize the frozen weights in Equations (8-9) once and save the quantized weights before fine-tuning. We then apply a single right-hand Hadamard transformation during the forward pass on the inputs and two Hadamard transformations during the backward pass on the errors. Finally, we keep the gradient calculation in high precision as it uses only low-rank matrix multiplication. We denote this variant scheme by **HALO_{PEFT}**.

5. Experimental Validation

Setup. We implement HALO in PyTorch (Paszke et al., 2019) using models from Hugging Face (Wolf et al., 2020). We use the llm-foundry (MosaicML, 2023) codebase for Full Fine-tuning (FFT), and the standard HuggingFace PEFT library for Parameter-Efficient Fine-Tuning (PEFT).

Throughout, we use **tensor-wise symmetric quantization** (a single scale for the entire tensor) for all data types using Round-to-Nearest (RTN). We implement our own low-precision matrix multiplications using the CUTLASS library (NVIDIA, 2017) for all linear modules (except for the LM head and embeddings) and keep the rest of the model in bfloat16 (BF16) during fine-tuning. As previously described, for outlier mitigation, we adapt the efficient CUDA kernels for Hadamard transformations (Dao, 2023b). We use E4M3 for the 8-bit floating-point format, and similarly, by comparing the final accuracy of various formats, we chose to use E3M2 for the 6-bit floating-point format.

Model and Tasks. For fine-tuning tasks, we evaluate our scheme on the standard LLAMA3-8Bmodel (Dubey et al., 2024). We have adopted this model since it has been extremely popular for fine-tuning. Consequently, highly accurate hyper-parameter recipes exist for fine-tuning it using different approaches across several challenging tasks (Artur et al., 2023; Nikdan et al., 2024).

We consider the following fine-tuning scenarios: 1) Full Fine-tuning (FFT where we update all parameters in the model, and 2) Parameter-Efficient Fine-Tuning (PEFT), specifically Low-Rank Adaptation (LoRA) (Hu et al., 2021), where we freeze the parameters of the linear modules and update a smaller (low-rank) set of parameters during the fine-tuning.

Method	Forward Calculation (F)	Input Gradient Calculation (E)	Weight Gradient Calculation (G)	Note
HALO-0(F, E, G)	$\mathbf{X}_Q \mathbf{W}_Q^T$	$(\mathbf{E}_Y)_Q \mathbf{W}_Q$	$(\mathbf{E}_Y^T)_Q \mathbf{X}_Q$	1. Most Efficient Scheme. 2. Suitable for wide ranges (e.g., FP8).
HALO-1($\overset{H}{F}$, $\overset{H}{E}$, $\overset{H}{G}$)	$(\mathbf{XH})_Q (\mathbf{WH})_Q^T$	$(\mathbf{E}_Y)_Q (\mathbf{WH})_Q \mathbf{H}^T$	$(\mathbf{E}_Y^T)_Q (\mathbf{XH})_Q \mathbf{H}^T$	1. Outlier mitigation during the forward pass. 2. Easy integration with FSDP with AC. 3. Quantized activation for memory reduction. 4. Suitable for moderate ranges (e.g., FP6).
HALO-2($\overset{H}{F}$, $\overset{H}{E}$, $\overset{H}{G}$)	$(\mathbf{XH})_Q (\mathbf{WH})_Q^T$	$\mathbf{H}^T (\mathbf{HE}_Y)_Q (\mathbf{WH})_Q \mathbf{H}^T$	$(\mathbf{E}_Y^T)_Q (\mathbf{XH})_Q \mathbf{H}^T$	1. Most accurate scheme. 2. Suitable for narrow ranges (e.g., INT8).

Table 1. HALO levels for full fine-tuning (FFT). We use the quantization function \mathbf{Q} for quantizing different data types and perform the computation with low precision. AC stands for Activation Checkpointing.

For both FFT and PEFT, we consider three standard datasets for fine-tuning:

- ViGGO (Juraska et al., 2019), with 5.1k training and 1.08k test samples,
- GSM8k (Cobbe et al., 2021), with 7.74k training and 1.32k test samples,
- SQL generation (Zhong et al., 2017; Yu et al., 2018), with 30k training and 1k test samples.

These datasets are particularly interesting because they are either specialized tasks (like SQL and ViGGO), or the pre-trained model has negligible few-shot accuracy (like GSM8K), making fine-tuning necessary.

Baselines. For full fine-tuning, we compare HALO against three main baselines: BF16, where no quantization is applied during forward and backward passes; SwitchBack (Wortsman et al., 2023); and Jetfire (Xi et al., 2024b), which both involve low-precision backward passes for training Transformer-based models. Unlike our scheme, neither method applies Hadamard transformations before quantization. SwitchBack uses row-wise quantization for the inputs and errors during the forward and backward passes and performs weight gradient calculation in 16 bits. For Jetfire, we apply 2D block-wise quantization with a block size of 32×32 on the linear layers and use symmetric AbsMax for quantization. Notably, for fair comparison, we maintain this scheme’s data flow in 16 bits and do not quantize the activation functions in our Jetfire baseline, as this aspect is orthogonal to our scheme. Finally, we will also compare HALO with the standard PEFT methods LoRA (Hu et al., 2021) with rank $r = 8$.

Hyper-parameters. In all cases, we tune the hyper-parameters on the base BF16 tasks, and re-use the same values for low-precision training. We always perform single-epoch experiments using the AdamW optimizer with $\beta_1 = 0.9$, $\beta_2 = 0.999$, and a linear learning rate warm-up of 20 steps. The batch size and sequence length are fixed at

32 and 512. For FFT, we choose learning rates 4×10^{-5} , 6×10^{-6} , and 3×10^{-5} for ViGGO, GSM8k, and SQL, respectively, and for PEFT LoRA experiments, we choose the learning rate 6×10^{-4} and LoRA rank of 16 for all datasets. These learning rates were found to be the best using a grid search within the range $[10^{-6}, 10^{-3}]$ of 20 uniform logarithmically separated grid points, trained and evaluated using the non-quantized BF16 training precision. We performed each experiment on 5 different seeds to report the mean and standard error of accuracy.

5.1. Low-Precision Full Fine-Tuning

Integer (INT8) Quantization. Table 2 summarizes the results of using HALO across three tasks, where weights, activations, and errors are quantized using symmetric INT8 quantization. We utilize the second level, denoted by HALO-2($\overset{H}{F}$, $\overset{H}{E}$, $\overset{H}{G}$), for integer quantization and compare our results against BF16 (no quantization), SwitchBack, and Jetfire. We observe the following:

- Across all tasks, HALO remains within a 1% relative accuracy range of the BF16 model, while using tensor-wise quantization for weights, inputs, and errors. It matches or improves the accuracy of other low-precision training methods, while having significantly lower variance across seeds.
- The more accurate variant of JetFire we compare against, with BF16 data flow, also falls within this range, but at the cost of using more fine-grained (32×32 block-wise) quantization.
- Finally, SwitchBack fails to recover accuracy in both the ViGGO and GSM8K datasets, even with row-wise and column-wise quantization of inputs and weights and high-precision weight gradient calculation. Notably, the SQL dataset appears to be “easier” under quantization, as all schemes can recover baseline accuracy with a single epoch of FFT.

Floating-Point Quantization. Next, we study the use of

Table 2. Single-epoch Full INT8 Fine-Tuning (FFT) accuracy comparison between BF16 FFT (no quantization), SwitchBack, and Jetfire. In this case, we use HALO-2($\overset{H}{F}$, $\overset{H}{E}$, $\overset{H}{G}$).

Precision	Method	GSM8k	ViGGO	SQL
BF16	Baseline	69.26 \pm 0.51	94.02 \pm 0.29	79.83 \pm 0.49
INT8	SwitchBack	63.97 \pm 0.74	61.0 \pm 28.86	79.58 \pm 0.76
	Jetfire	68.23 \pm 0.59	93.64 \pm 0.40	80.18 \pm 0.58
	HALO-2	68.15 \pm 0.08	93.79 \pm 0.08	80.12 \pm 0.31

floating-point representation during fine-tuning by applying FP6 (E3M2) and FP8 (E4M3) quantization. For FP6, we utilize the first level, denoted by HALO-1($\overset{H}{F}$, $\overset{H}{E}$, $\overset{H}{G}$), where we apply the Hadamard transform on the forward pass and use the Hadamard-transformed weights and inputs during the backward calculation. We note that, although the peak performance of FP6 is the same as FP8 in NVIDIA GPU architectures (NVIDIA, 2024), FP6 provides higher memory and communication reduction with quantized activations and HQ-FSDP. For FP8, we do not apply any Hadamard transformation in our experiments, and employ the basic HALO-0(F , E , G) variant.

Table 3. Single-epoch accuracy results of fine-tuning with 8-bit and 6-bit floating-point quantizations. For FP6 (E3M2), we use the HALO-1($\overset{H}{F}$, $\overset{H}{E}$, $\overset{H}{G}$) while we use no Hadamard for FP8 (E4M3), denoted by HALO-0(F , E , G).

Precision	Method	GSM8k	ViGGO	SQL
BF16	Baseline	69.26 \pm 0.51	94.02 \pm 0.29	79.83 \pm 0.49
FP6	SwitchBack	62.71 \pm 0.70	93.39 \pm 0.49	80.06 \pm 0.52
	Jetfire	62.80 \pm 1.10	92.94 \pm 0.16	79.74 \pm 0.54
	HALO-1	66.54 \pm 0.22	93.56 \pm 0.38	80.20 \pm 0.26
FP8	HALO-0	69.21 \pm 0.21	93.13 \pm 0.28	80.33 \pm 0.05

Table 3 shows the results of FP6 and FP8 quantization. On the GSM8K dataset, both SwitchBack and Jetfire have approximately 6.5% accuracy drop, while HALO-1 shows a 2.7% accuracy loss compared to the BF16 model. On the ViGGO dataset, HALO experiences a 0.46% accuracy drop, whereas SwitchBack and Jetfire show drops of 0.63% and 1.1%, respectively. Similar to integer quantization, all methods achieve accuracy within 1% of the baseline on the SQL dataset.

5.2. Low-Precision PEFT

We now evaluate HALO on PEFT, where we fine tune LLAMA3-8B on GSM8K, SQL, and ViGGO datasets. We compare our PEFT scheme, denoted by HALO_{PEFT}, against LoRA (Hu et al., 2021). We apply both FP6 and INT8 during fine-tuning for our scheme.

Table 4 presents the results of applying HALO during

Table 4. Single-epoch accuracy comparison between LoRA (Hu et al., 2021) and HALO_{PEFT}(ours). We use rank $r = 16$ for adapters and apply FP6 (E3M2) and INT8 for quantization.

Precision	Method	GSM8k	ViGGO	SQL
BF16	LoRA	69.40 \pm 0.76	94.09 \pm 0.21	79.90 \pm 0.40
INT8	HALO _{PEFT}	68.98 \pm 0.46	93.39 \pm 0.65	79.94 \pm 0.36
FP6	HALO _{PEFT}	67.28 \pm 0.64	93.59 \pm 0.70	79.88 \pm 0.46

PEFT with INT8 and FP6 precisions. When using INT8, HALO_{PEFT} performs within the standard deviation of the BF16 model across all datasets. On GSM8K, FP6 has approximately a 2% accuracy degradation, showing the challenge of recovering high-precision accuracy with only 6 bits. For the ViGGO and SQL datasets, both INT8 and FP6 recover accuracy with at most a 0.5% average accuracy drop. Compared to FFT, HALO has a smaller accuracy gap from the BF16 model during PEFT with INT8 quantization.

5.3. Speedup Analysis

In this section, we evaluate the runtime improvements achieved with HALO. Speedups are measured on RTX 4090 GPUs with locked clocks, to reduce variance, for: (1) a single Linear layer, (2) three Transformer blocks (with and without FSDP), and (3) end-to-end training. We compare different precisions and HALO levels against the BF16 base case and other baselines. We fix the sequence length at 512 and control the input size using the batch size. The module-level and block-level speedups are averaged over 100 (+20 warm-up) and 30 (+10 warm-up) runs, respectively.

INT8 Linear Layer. In this runtime experiment, we consider a single linear layer of size 4096×4096 , which is present in the majority of linear blocks in the LLAMA3-8B model, and our best-performing INT8 quantization scheme in terms of accuracy, HALO-2($\overset{H}{F}$, $\overset{H}{E}$, $\overset{H}{G}$), with Jetfire (Xi et al., 2024b) and SwitchBack (Wortsmann et al., 2023). Since Jetfire uses an INT8 data flow, we consider a setup where its inputs, outputs, and errors are in INT8, partially bypassing quantization overhead by quantizing only the weights on the fly. (We use this idealized version of Jetfire to ensure a fair comparison.)

Figure 4 illustrates the speedups relative to the baseline BF16 implementation. We observe that, for batch sizes greater than 4, HALO-2 performs nearly on par with Jetfire (between $1.4\times$ and $1.6\times$), despite Jetfire’s lower quantization overhead due to its INT8 data flow. Integrating our method with low-precision data flow could further enhance speedup. We leave this for future work.

Transformer Blocks. In Figure 5, we repeat the previous INT8 experiment on three consecutive transformer blocks

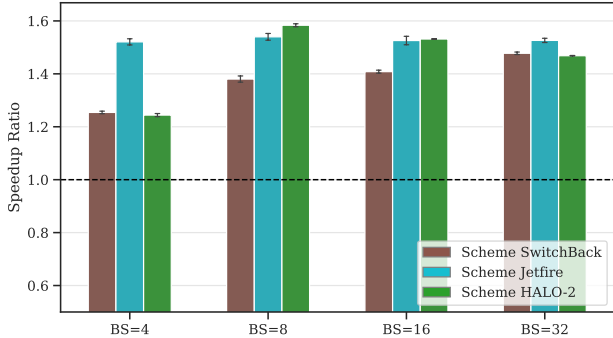


Figure 4. Forward + Backward layer-wise INT8 speedups for different batch sizes (BS). The layer size is 4096 and the sequence length is 512. HALO-2 refers to HALO-2($\mathbf{F}^H, \mathbf{E}^H, \mathbf{G}^H$).

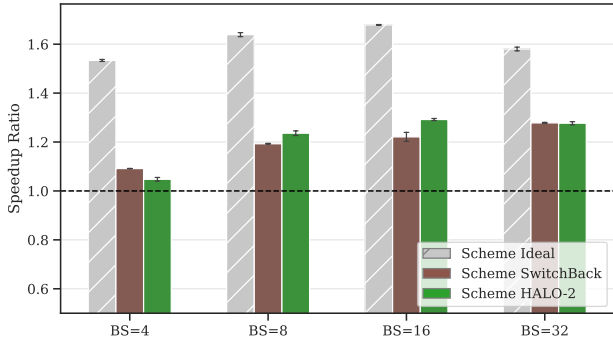


Figure 5. Forward + Backward INT8 speedups for different batch sizes (BS) on three consecutive blocks of LLAMA3-8B. The sequence length is 512. HALO-0 and HALO-1 refer to HALO-0($\mathbf{F}, \mathbf{E}, \mathbf{G}$) and HALO-1($\mathbf{F}^H, \mathbf{E}^H, \mathbf{G}^H$), respectively.

taken from LLAMA3-8B (Dubey et al., 2024) (this is the largest number of blocks that fit on one GPU with batch size 32). Jetfire is excluded from this comparison since its non-linear operations are performed with INT8 inputs, making a fair comparison impossible. This figure also includes an *ideal* speedup, where all Hadamard transforms are removed and the quantization is replaced with a simple INT8 casting. The large gap between the ideal speedup and HALO-2 is due to the Hadamard transforms and quantization overheads in this HALO level, suggesting that our implementation can be further optimized. Yet, HALO-2 slightly outperforms SwitchBack for batch sizes over 4 and, as shown in Table 2, consistently achieves higher accuracy.

We also benchmark HALO-0($\mathbf{F}, \mathbf{E}, \mathbf{G}$) and HALO-1($\mathbf{F}^H, \mathbf{E}^H, \mathbf{G}^H$) with FP8 quantization in Figure 6. HALO-0 is nearly on par with ideal speedup, peaking at $1.35\times$. For HALO-1, we note that it should ideally run with FP6 quantization. However, since hardware support for FP6 matrix multiplication is unavailable, we use FP8 matmul instead to provide a lower bound on the FP6 speedup, which peaks at $1.22\times$.

The Effect of HQ-FSDP. To evaluate the impact of HQ-FSDP, we revisit the experiment with three consecutive

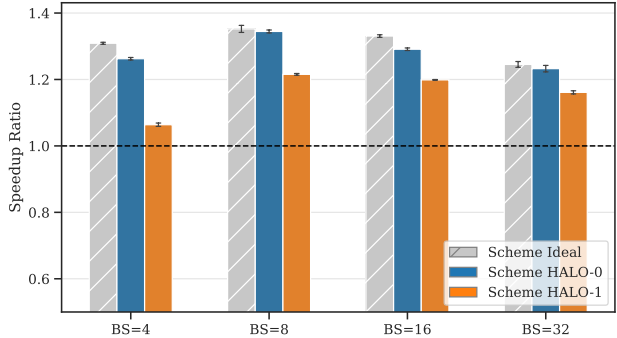


Figure 6. Forward + Backward FP8 speedups for different batch sizes (BS) on three consecutive blocks of LLAMA3-8B. The sequence length is 512, and HALO-2 refers to HALO-2($\mathbf{F}^H, \mathbf{E}^H, \mathbf{G}^H$).

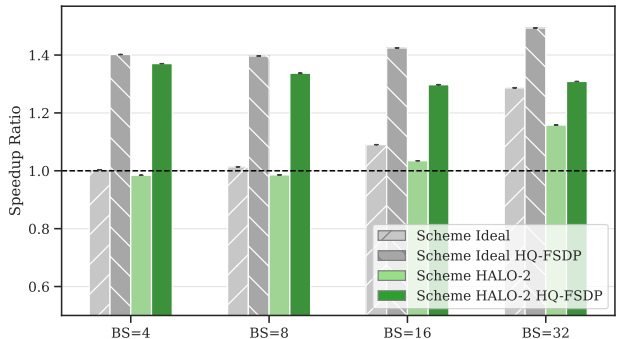


Figure 7. Forward + Backward INT8 speedups with and without HQ-FSDP for different batch sizes (BS) on three consecutive blocks of LLAMA3-8B. The sequence length is 512. HALO-0 and HALO-1 refer to HALO-0($\mathbf{F}, \mathbf{E}, \mathbf{G}$) and HALO-1($\mathbf{F}^H, \mathbf{E}^H, \mathbf{G}^H$), respectively.

transformer blocks, this time using four GPUs with FSDP enabled. Speedup results are reported with and without quantized communication. To minimize communication overhead, 64 NCCL threads are used (optimized through tuning) and forward and backward prefetching are activated. Figures 7 and 8 show the results for INT8 and FP8 cases, respectively. The figures consistently show that without HQ-FSDP, communication overhead significantly reduces speedups, while with quantized communication, we achieve speedups between $1.2\times$ and $1.4\times$. This means HQ-FSDP plays a crucial role in achieving end-to-end training speedups, which we will measure next. An interesting observation is that with HQ-FSDP, the highest speedup occurs at a batch size of 4. This is because, as the batch size decreases, the communication overhead becomes the bottleneck. Consequently, the reduction in communication overhead has a more significant impact on the overall speedup.

End-to-End Speedups. Finally, we examine the end-to-end fine-tuning speedups for LLAMA3-8B using FP8 HALO-0 and INT8 HALO-2, both of which are near-

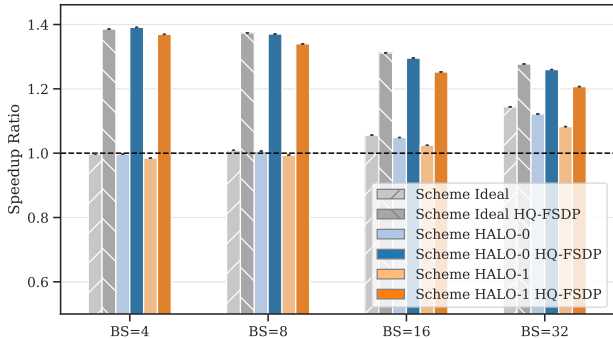


Figure 8. Forward + Backward FP8 speedups with and without HQ-FSDP for different batch sizes (BS) on three consecutive blocks of LLAMA3-8B. The sequence length is 512, and HALO-2 refers to HALO-2($\overset{H}{F}$, $\overset{H}{E}^H$, $\overset{H}{G}^H$).

lossless for the corresponding precisions. The experiments are performed in a realistic setting with four GPUs, with HQ-FSDP and Activation Checkpointing enabled. The sequence length is set to 512, and the micro-batch size is 4. In this setting, we get end-to-end training speedups of $1.29\times$ and $1.31\times$ for INT8 and FP8, respectively.

5.4. Ablation Study on HALO Levels

One interesting question concerns the comparison between the different levels of HALO introduced in Section 4.3, that is HALO-0($\overset{H}{F}$, $\overset{H}{E}$, $\overset{H}{G}$), HALO-1($\overset{H}{F}$, $\overset{H}{E}^H$, $\overset{H}{G}^H$), and HALO-2($\overset{H}{F}$, $\overset{H}{E}^H$, $\overset{H}{G}^H$) used during the fine-tuning of FP8, FP6, and INT8, respectively.

Table 5 shows the effect of using different levels for INT8 and FP6, illustrating the natural finding that a higher HALO level results in higher final test accuracy. For INT8 precision, HALO-0 fails to recover accuracy, leading to an approximate 40% drop in accuracy (on average) on our datasets. At the next level, HALO-1 recovers approximately 37% of the above accuracy gap by applying right-hand-side Hadamard transformations on the weights and inputs during both the forward and backward passes. Finally, HALO-2 applies left-hand-side Hadamard transformations on the errors, achieving within 1% of the BF16 accuracy. For FP6 precision, although HALO-2 achieves higher accuracy on the GSM8K dataset, believe HALO-1 provides a better trade-off between accuracy and the number of Hadamard transformations.

6. Conclusion

In this paper, we introduced HALO, a low-precision LLM fine-tuning scheme that uses the Hadamard transformation to mitigate outliers during quantized training. Specifically, HALO works by addressing the algorithmic and system challenges of using low-precision matrix multiplication during the fine-tuning of such models by judiciously placing

Table 5. The accuracy effects of using different HALO levels within each quantization precision. The selected level for each precision is presented with **bold** text. We exclude FP8 experiments as HALO-0 recovers the BF16 accuracy.

Precision	Method	GSM8k	ViGGO	SQL
BF16	Baseline	69.26 ± 0.51	94.02 ± 0.29	79.83 ± 0.49
FP6	HALO-0	62.32 ± 0.65	92.92 ± 0.73	79.24 ± 0.36
	HALO-1	66.54 ± 0.22	93.56 ± 0.38	80.20 ± 0.26
	HALO-2	67.42 ± 0.99	93.56 ± 0.38	80.00 ± 0.62
INT8	HALO-0	4.50 ± 1.03	55.98 ± 20.89	74.73 ± 0.45
	HALO-1	62.27 ± 0.64	93.23 ± 0.45	79.43 ± 0.59
	HALO-2	68.15 ± 0.08	93.79 ± 0.08	80.12 ± 0.31

Hadamard transformations in the forward and backward passes. HALO uses simple tensor-wise quantization for all weights, inputs, and errors, utilizes low-precision communication (HQ-FSDP), and reduces memory usage by storing quantized activations. We also present different levels of applying Hadamard transformations for various data types, including INT8, FP6, and FP8. Using INT8 and FP8, HALO can achieve $1.29\times$ and $1.31\times$ end-to-end speedups, respectively, for fine-tuning LLAMA3-8B on four consumer-type GPUs while maintaining close-to-baseline accuracy.

References

- Artur, N., Kourosh, H., and Rehaan, A. Fine-tuning llms: Lora or full-parameter? an in-depth analysis with llama 2. <https://www.anyscale.com/blog?author=rehaan-ahmad>, 2023.
- Ashkboos, S., Markov, I., Frantar, E., Zhong, T., Wang, X., Ren, J., Hoefler, T., and Alistarh, D. Towards end-to-end 4-bit inference on generative large language models. *arXiv preprint arXiv:2310.09259*, 2023.
- Ashkboos, S., Mirzadeh, I., Alizadeh, K., Sekhavat, M. H., Nabi, M., Farajtabar, M., and Faghri, F. Computational bottlenecks of training small-scale large language models. *arXiv preprint arXiv:2410.19456*, 2024a.
- Ashkboos, S., Mohtashami, A., Croci, M. L., Li, B., Jaggi, M., Alistarh, D., Hoefler, T., and Hensman, J. Quarot: Outlier-free 4-bit inference in rotated llms. *arXiv preprint arXiv:2404.00456*, 2024b.
- Baalen, M. v., Kuzmin, A., Nair, S. S., Ren, Y., Mahurin, E., Patel, C., Subramanian, S., Lee, S., Nagel, M., Soriaga, J., et al. Fp8 versus int8 for efficient deep learning inference. *arXiv preprint arXiv:2303.17951*, 2023.
- Chee, J., Cai, Y., Kuleshov, V., and De Sa, C. M. Quip: 2-bit quantization of large language models with guarantees. *Advances in Neural Information Processing Systems*, 36, 2024.

- Chen, Y., Jalali, A., Sanghavi, S., and Xu, H. Incoherence-optimal matrix completion. *arXiv preprint arXiv:1310.0154*, 2013. Available at <https://arxiv.org/abs/1310.0154>.
- Chitsaz, K., Fournier, Q., Mordido, G., and Chandar, S. Exploring quantization for efficient pre-training of transformer language models. *arXiv preprint arXiv:2407.11722*, 2024.
- Cobbe, K., Kosaraju, V., Bavarian, M., Chen, M., Jun, H., Kaiser, L., Plappert, M., Tworek, J., Hilton, J., Nakano, R., Hesse, C., and Schulman, J. Training verifiers to solve math word problems. *arXiv preprint arXiv:2110.14168*, 2021.
- Dao, T. Flashattention-2: Faster attention with better parallelism and work partitioning. *arXiv preprint arXiv:2307.08691*, 2023a.
- Dao, T. Fast hadamard transform in cuda, 2023b. URL <https://github.com/Dao-AILab/fast-hadamard-transform>.
- Dettmers, T., Lewis, M., Belkada, Y., and Zettlemoyer, L. Gpt3.int8(): 8-bit matrix multiplication for transformers at scale. *Advances in Neural Information Processing Systems*, 35:30318–30332, 2022.
- Dettmers, T., Svirschevski, R., Egiazarian, V., Kuznedelev, D., Frantar, E., Ashkboos, S., Borzunov, A., Hoefler, T., and Alistarh, D. Spqr: A sparse-quantized representation for near-lossless llm weight compression. *arXiv preprint arXiv:2306.03078*, 2023.
- Dettmers, T., Pagnoni, A., Holtzman, A., and Zettlemoyer, L. Qlora: Efficient finetuning of quantized llms. *Advances in Neural Information Processing Systems*, 36, 2024.
- Dubey, A., Jauhri, A., Pandey, A., Kadian, A., Al-Dahle, A., Letman, A., Mathur, A., Schelten, A., Yang, A., Fan, A., et al. The llama 3 herd of models. *arXiv preprint arXiv:2407.21783*, 2024.
- Egiazarian, V., Panferov, A., Kuznedelev, D., Frantar, E., Babenko, A., and Alistarh, D. Extreme compression of large language models via additive quantization. *arXiv preprint arXiv:2401.06118*, 2024.
- Fishman, M., Chmiel, B., Banner, R., and Soudry, D. Scaling fp8 training to trillion-token llms. *arXiv preprint arXiv:2409.12517*, 2024.
- Flashinfer.ai. Flashinfer: Kernel library for llm serving, 2023. URL <https://github.com/flashinfer-ai/flashinfer>.
- Frantar, E., Ashkboos, S., Hoefler, T., and Alistarh, D. GPTQ: Accurate post-training quantization for generative pre-trained transformers. *arXiv preprint arXiv:2210.17323*, 2022.
- Hu, E. J., Shen, Y., Wallis, P., Allen-Zhu, Z., Li, Y., Wang, S., Wang, L., and Chen, W. Lora: Low-rank adaptation of large language models. *arXiv preprint arXiv:2106.09685*, 2021.
- Juraska, J., Bowden, K., and Walker, M. ViGGO: A video game corpus for data-to-text generation in open-domain conversation. In *Proceedings of the 12th International Conference on Natural Language Generation*, pp. 164–172, Tokyo, Japan, October–November 2019. Association for Computational Linguistics. doi: 10.18653/v1/W19-8623. URL <https://aclanthology.org/W19-8623>.
- Kwon, W., Li, Z., Zhuang, S., Sheng, Y., Zheng, L., Yu, C. H., Gonzalez, J., Zhang, H., and Stoica, I. Efficient memory management for large language model serving with pagedattention. In *Proceedings of the 29th Symposium on Operating Systems Principles*, pp. 611–626, 2023.
- LeCun, Y., Bottou, L., Orr, G. B., and Müller, K.-R. Efficient backprop. In *Neural networks: Tricks of the trade*, pp. 9–50. Springer, 2002.
- Liu, Z., Zhao, C., Fedorov, I., Soran, B., Choudhary, D., Krishnamoorthi, R., Chandra, V., Tian, Y., and Blankevoort, T. Spinquant-llm quantization with learned rotations. *arXiv preprint arXiv:2405.16406*, 2024.
- Micikevicius, P., Narang, S., Alben, J., Diamos, G., Elsen, E., Garcia, D., Ginsburg, B., Houston, M., Kuchaiev, O., Venkatesh, G., et al. Mixed precision training. *arXiv preprint arXiv:1710.03740*, 2017.
- MosaicML. Llm training code for databricks foundation models, 2023. URL <https://github.com/mosaicml/llm-foundry>.
- Nikdan, M., Tabesh, S., and Alistarh, D. Rosa: Accurate parameter-efficient fine-tuning via robust adaptation. *arXiv preprint arXiv:2401.04679*, 2024.
- Nrusimha, A., Mishra, M., Wang, N., Alistarh, D., Panda, R., and Kim, Y. Mitigating the impact of outlier channels for language model quantization with activation regularization, 2024. URL <https://arxiv.org/abs/2404.03605>.
- NVIDIA. Cutlass: Cuda templates for linear algebra subroutines, 2017. URL <https://github.com/NVIDIA/cutlass>.

- NVIDIA. Nvidia blackwell architecture technical brief. "<https://resources.nvidia.com/en-us-blackwell-architecture>", 2024.
- Paszke, A., Gross, S., Massa, F., Lerer, A., Bradbury, J., Chanan, G., Killeen, T., Lin, Z., Gimelshein, N., Antiga, L., et al. Pytorch: An imperative style, high-performance deep learning library. *Advances in neural information processing systems*, 32, 2019.
- Peng, H., Wu, K., Wei, Y., Zhao, G., Yang, Y., Liu, Z., Xiong, Y., Yang, Z., Ni, B., Hu, J., et al. Fp8-lm: Training fp8 large language models. *arXiv preprint arXiv:2310.18313*, 2023.
- Sun, M., Chen, X., Kolter, J. Z., and Liu, Z. Massive activations in large language models. *arXiv preprint arXiv:2402.17762*, 2024.
- Tseng, A., Chee, J., Sun, Q., Kuleshov, V., and De Sa, C. Quip#: Even better llm quantization with hadamard incoherence and lattice codebooks. *arXiv preprint arXiv:2402.04396*, 2024.
- Vaswani, A. Attention is all you need. *Advances in Neural Information Processing Systems*, 2017.
- Wei, X., Zhang, Y., Zhang, X., Gong, R., Zhang, S., Zhang, Q., Yu, F., and Liu, X. Outlier suppression: Pushing the limit of low-bit transformer language models. *Advances in Neural Information Processing Systems*, 35:17402–17414, 2022.
- Wolf, T., Debut, L., Sanh, V., Chaumond, J., Delangue, C., Moi, A., Cistac, P., Rault, T., Louf, R., Funtowicz, M., et al. Transformers: State-of-the-art natural language processing. In *Proceedings of the 2020 conference on empirical methods in natural language processing: system demonstrations*, pp. 38–45, 2020.
- Wortsman, M., Dettmers, T., Zettlemoyer, L., Morcos, A., Farhadi, A., and Schmidt, L. Stable and low-precision training for large-scale vision-language models. *Advances in Neural Information Processing Systems*, 36: 10271–10298, 2023.
- Xi, H., Li, C., Chen, J., and Zhu, J. Training transformers with 4-bit integers. *Advances in Neural Information Processing Systems*, 36:49146–49168, 2023.
- Xi, H., Cai, H., Zhu, L., Lu, Y., Keutzer, K., Chen, J., and Han, S. Coat: Compressing optimizer states and activation for memory-efficient fp8 training. *arXiv preprint arXiv:2410.19313*, 2024a.
- Xi, H., Chen, Y., Zhao, K., Zheng, K., Chen, J., and Zhu, J. Jetfire: Efficient and accurate transformer pretraining with int8 data flow and per-block quantization. *arXiv preprint arXiv:2403.12422*, 2024b.
- Xiao, G., Lin, J., Seznec, M., Wu, H., Demouth, J., and Han, S. Smoothquant: Accurate and efficient post-training quantization for large language models. In *International Conference on Machine Learning*, pp. 38087–38099. PMLR, 2023.
- Yavne, R. An economical method for calculating the discrete fourier transform. In *Proceedings of the December 9-11, 1968, fall joint computer conference, part I*, pp. 115–125, 1968.
- Yu, T., Zhang, R., Yang, K., Yasunaga, M., Wang, D., Li, Z., Ma, J., Li, I., Yao, Q., Roman, S., et al. Spider: A large-scale human-labeled dataset for complex and cross-domain semantic parsing and text-to-sql task. *arXiv preprint arXiv:1809.08887*, 2018.
- Zhao, Y., Gu, A., Varma, R., Luo, L., Huang, C.-C., Xu, M., Wright, L., Shojanazeri, H., Ott, M., Shleifer, S., et al. Pytorch fsdp: experiences on scaling fully sharded data parallel. *arXiv preprint arXiv:2304.11277*, 2023a.
- Zhao, Y., Lin, C.-Y., Zhu, K., Ye, Z., Chen, L., Zheng, S., Ceze, L., Krishnamurthy, A., Chen, T., and Kasikci, B. Atom: Low-bit quantization for efficient and accurate llm serving. *arXiv preprint arXiv:2310.19102*, 2023b.
- Zhong, V., Xiong, C., and Socher, R. Seq2sql: Generating structured queries from natural language using reinforcement learning. *CoRR*, abs/1709.00103, 2017.

A. Appendix

A.1. HQ-FSDP Details

Here we discuss some details about our HQ-FSDP implementation.

Master Weights. In HALO, weights are maintained in BF16. Accordingly, HQ-FSDP stores the parameters in BF16 and applies quantization before communication.

Forward vs. Backward. Since the weights remain unchanged between the forward and backward passes, the quantized shard could be stored during the forward pass in each process and only communicated during the backward pass. This approach eliminates the need for a second quantization and potential Hadamard transform during the backward pass. However, it introduces additional memory overhead, as the quantized weights must be stored alongside the master BF16 weights. Additionally, since the quantization and Hadamard transform on the weights are distributed across FSDP processes, their overhead is relatively small. Instead, we adopt an intermediate approach: save only the global quantization scales during the forward pass and recompute the quantization and Hadamard transform during the backward pass.

FSDP Wrapping Policy. Following standard practice, we wrap each transformer block with an FSDP module (FSDP communications happen before each transformer block). However, for HQ-FSDP, we skip the layer-norm modules (keeping full weights in every process) as we do not intend to quantize them. Our experiments show that this only marginally increases memory usage and does not change runtime.

Distributed Hadamard Transformation. When the scheme requires a right Hadamard transformation, HQ-FSDP applies it in a distributed way; process i performs $\mathbf{W}_i\mathbf{H}$ where \mathbf{W}_i denotes the i 'th shard. However, this requires the weight matrix to be sharded by row, i.e., each row should entirely reside within a single shard. As FSDP requires equally sized shards to be fast, we dynamically insert small dummy parameter tensors of carefully chosen sizes when needed. This guarantees row-aligned sharding without compromising performance.